

Open Rotor Noise Shielding by Blended-Wing-Body Aircraft

Yueping Guo*

Boeing Research & Technology, Huntington Beach, CA 92647 USA

Michael J. Czech†

Boeing Commercial Airplane, P.O. Box 3707, Everett, WA 98204 USA

and

Russell H. Thomas‡

NASA Langley Research Center, Hampton, VA 23681 USA

This paper presents an analysis of open rotor noise shielding by Blended Wing Body (BWB) aircraft by using model scale test data acquired in the Boeing Low Speed Aeroacoustic Facility (LSAF) with a legacy F7/A7 rotor model and a simplified BWB platform. The objective of the analysis is the understanding of the shielding features of the BWB and the method of application of the shielding data for noise studies of BWB aircraft with open rotor propulsion. By studying the directivity patterns of individual tones, it is shown that though the tonal energy distribution and the spectral content of the wind tunnel test model, and thus its total noise, may differ from those of more advanced rotor designs, the individual tones follow directivity patterns that characterize far field radiations of modern open rotors, ensuring the validity of the use of this shielding data. Thus, open rotor tonal noise shielding should be categorized into front rotor tones, aft rotor tones and interaction tones, not only because of the different directivities of the three groups of tones, but also due to the differences in their source locations and coherence features, which make the respective shielding characteristics of the three groups of tones distinctly different from each other. To reveal the parametric trends of the BWB shielding effects, results are presented with variations in frequency, far field emission angle, rotor operational condition, engine installation geometry, and local airframe features. These results prepare the way for the development of parametric models for the shielding effects in prediction tools.

Nomenclature

<i>BPF</i>	=	blade passage frequency
<i>BWB</i>	=	Blended-Wing-Body, Boeing specific design
<i>D</i>	=	rotor diameter
<i>dB</i>	=	decibel
<i>ERA</i>	=	NASA's Environmentally Responsible Aviation Project
<i>EPNL</i>	=	effective perceived noise level, decibels
<i>HWB</i>	=	Hybrid Wing Body, generic term
<i>LSAF</i>	=	Low Speed Aeroacoustic Facility, Boeing
<i>M</i>	=	mean flow Mach number
<i>PNLT</i>	=	tone corrected perceived noise level, decibels
<i>SPL</i>	=	sound pressure level

* Technical Fellow, Acoustics Technology, 5301 Bolsa Ave, Huntington Beach, CA, AIAA Associate Fellow, Current Address: NEAT Consulting, 3830 Daisy Circle, Seal Beach, CA 90740

† Engineer, Acoustics Technology, P.O. Box 3707, MC OR-JF, Seattle, WA

‡ Senior Research Engineer, Aeroacoustics Branch, MS 461, AIAA Senior Member

I. Introduction

In order to achieve both low noise and high fuel efficiency, the combination of a Hybrid Wing Body (HWB) or Blended Wing Body (BWB) airframe and open rotor engines presents a promising aircraft concept. With the engines mounted on the upper surface of the aircraft to provide community noise reduction through shielding and with the open rotor engines providing the fuel efficiency, the BWB concept with open rotors may provide these simultaneous benefits. To understand the noise characteristics of such airframe/engine design combination and to provide data for the assessment and modeling of the shielding effects, an experimental study was conducted in the Boeing Low Speed Aeroacoustic Facility (LSAF), using the legacy F7/A7 open rotor model (Ref 1) and a simplified BWB aircraft planform model (Ref 2). In this paper, an analysis is presented to reveal the noise shielding effects and their parametric trends in frequency, far field emission angle, tone type, engine power setting, engine location, and configuration changes of the BWB airframe model, including vertical tails and local airframe surface liner treatments. These parametric trends can not only provide the understanding for the development of prediction models, but can also be directly used in system noise studies for BWB aircraft with open rotor propulsion (Ref 3-5).

It is known that open rotor noise is dominated by tones with spectral features and amplitude distributions determined by the detailed rotor design and operating conditions. Thus, it is difficult to claim similarity in noise characteristics between a wind tunnel test model and full scale configurations, unless the wind tunnel model is a precise scale-down of the full configuration design, operating at precisely scaled conditions. In practical applications, wind tunnel test models will likely differ from full configuration designs, as is the case of the LSAF test that used a pre-existing F7/A7 open rotor model with a very different design from the state of current technology. The lack of similarity in total engine noise characteristics then raises the question of how wind tunnel data can be utilized for full scale engines of different designs, and more generally, how open rotor noise shielding can be studied and applied. Clearly, the shielding effects, namely, noise reduction, cannot be applied in 1/3 octave bands, as is commonly done for broadband noise such as jet noise from turbofan engines (Ref 5-7), because the spectral contents of open rotor noise within the 1/3 octave bands can be different for different rotor designs.

Instead, it is proposed in this paper that the shielding effects need to be applied on individual tones, in a similar way to the application of narrow band liner noise suppression for turbofan engine tones. Furthermore, the tonal shielding effects need to be categorized in three different groups, namely, the front rotor tones, the aft rotor tones and the interaction tones, because the three groups have drastically different shielding characteristics. It will be shown that for all three groups, zones under the aircraft with heavy noise shielding can be determined from the principles of geometric acoustics (Ref 8, 9) according to the respective source locations of the tones. The levels of noise reduction in these shielded zones, however, depend not only on the source locations, but also the tonal directivity and source coherence. As a result, the aft rotor tones experience much less shielding than the front rotor tones, by more than 6 dB for the low and intermediate order tones, even though the sources of the two groups of tones are separated by only a small distance. It will also be shown that the shielding for the interaction tones is heavy and approximately uniform in frequency, lacking the interference pattern and frequency dependent diffraction typically associated with coherent sources. These shielding features will be analyzed and discussed from the tone generation mechanisms, the radiation patterns and the source coherence. It is these features that call for the categorization of the three groups of tones in studying and applying noise shielding for open rotor engines.

In this tonal approach of categorizing individual tones into various groups in open rotor noise shielding studies, the wind tunnel test results are considered as a collection of tonal shielding effects, while the overall rotor design and its total noise characteristics are less of a concern. Furthermore, for noise shielding effects that deal with differences in noise levels, not the absolute amplitudes, the radiation directivities of the tones for the isolated rotors critically determine the shielding characteristics. For example, maximum shielding can be expected if the BWB airframe blocks the peak radiation directions of the tones. On the other hand, the shielding effects will be limited if the trailing edges of the BWB airframe are exposed to the peak directions of the tonal directivities, because the acoustic energy incident on the edges will be maximal, which in turn will cause maximal diffraction into the shielded zones, effectively diverting the high acoustic energy in the tonal peak radiation directions to other angles. Clearly, the tonal directivities play a critical role in these features, and it is important to ensure the tonal directivities of the wind tunnel test model correctly capture those of full configuration rotor engines. To this end, the directivities of the three groups of tones from the wind tunnel model will be compared with those expected for more advanced and more recent rotor designs, showing good agreement between the two.

To further reveal the parametric trends in noise reduction due to BWB shielding, parametric studies will be presented to demonstrate the impact of various design changes that are possible with the integration of the BWB airframe and open rotor engines. These include the variations in the engine locations that have a direct impact on the noise shielding efficiency, especially the engine positions in relation to the BWB trailing edges. It will be shown that

the rotor positions determine the ranges and angles of the shielded zones, as well as the levels of noise reduction inside these zones. These features will be quantified by the analysis. Local design features of the BWB airframe such as vertical control surfaces will be considered, which may impact the total noise shielding effect, and the concept of acoustic liner treatment on the BWB airframe surface that may absorb the acoustic wave impinging on the surfaces will also be studied. It will be shown that these concepts all have the potential to reduce noise, and the noise reduction will be quantified as a function of the design parameters.

While the main objective of the paper is to understand the essential shielding characteristics of open rotor engines and to provide data for system noise assessment and prediction tool development, it is important to emphasize two aspects in discussing the results of tonal shielding and the noise reduction concepts. The first is the impact of the shielding or reduction of the tones to the total aircraft noise levels. The tonal shielding will be shown to be very significant, more than 20 dB in some cases, but the total aircraft noise reduction due to shielding can be expected to be much less, as demonstrated in Ref 3-6, because total aircraft noise is measured with many other components that are not affected by shielding. Furthermore, the total aircraft noise, the Effective Perceived Noise Level (EPNL) for aircraft noise certification, for example, is an aggregate measure of the noise in all radiation angles and all frequencies, some of which may not benefit from shielding, and thus holding up the overall noise levels. The second aspect to emphasize is the practical feasibility of the shielding and noise reduction concepts. Some of the concepts are only in their early stage of research, and some may not be feasible or favorable in aircraft design even when the technologies are mature, because of their potential adverse impact on aircraft performance. For example, engine locations upstream of the BWB trailing edge further than one rotor diameter will be shown to significantly enhance noise shielding, but it could unacceptably degrade the aerodynamic propulsion integration. Similarly, vertical control surfaces located next to the engines will be shown to be beneficial to sideline noise shielding, but they may cost extra fuel for the added weight. Aircraft weight and fuel cost are critical design criteria, and the trade between a few dB of noise reduction and a few percent of fuel cost would be considered only if the gain in noise reduction is absolutely necessary either in meeting regulatory requirements or for competitive reasons.

II. Experimental Setup

The details of the LSAF test were described in Ref 2 so that only a brief introduction is given here to facilitate the discussions in the following sections. The test facility is the Low Speed Aeroacoustic Facility (LSAF) at Boeing, as schematically shown in Figure 1, which is an open flow anechoic wind tunnel with a nominal test section of 9 feet by 12 feet in size. The flow Mach number can vary from 0.05 to 0.25. The mean flow and the test section are inside an anechoic chamber that is 65 feet long, 75 feet wide and 30 feet high. The anechoic chamber has good acoustic properties in the frequency range between 200 Hz and 80,000 Hz. The free jet flow is supplied by two centrifugal fans operating in parallel, with a combined flow of 2000 pounds per second at the Mach 0.25 design point. Each fan has a 107-inch wheel with backward inclined airfoil blades, and is powered by a 5200 horsepower synchronous motor. Tunnel speed is controlled by variable frequency motor speed controls, operating remotely from the LSAF control room, over a range of $M = 0.05$ to 0.25. The free jet exhaust is through a 19-foot square (361 square feet) exhaust area.

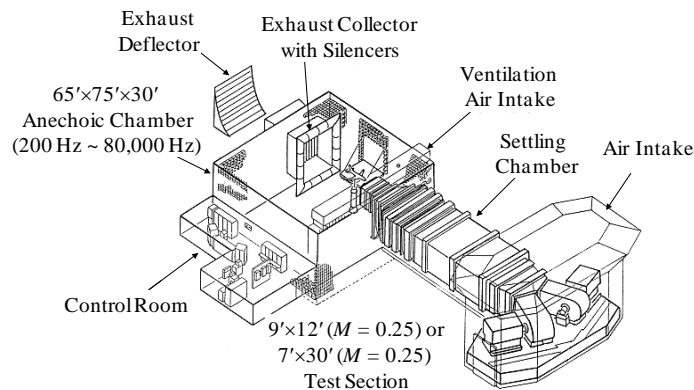


Figure 1. Boeing's Low Speed Aeroacoustic Facility (LSAF).

The test article is a combination of an open rotor model and a BWB airframe planform model. The open rotor model is the legacy F7/A7 design, with 8 blades for both the front and the aft rotor, both being of the same diameter of 12 inches. The isolated rotor model is shown in Figure 2 as installed in the LSAF test section, with its own pylon

and the supporting strut which encloses the high pressure air supply system. The rotors were operated at different speeds, typically with the aft rotor about 10 percent faster than the front rotor, so that the rotor tones and the interaction tones can be easily distinguished (Table 1). The rotor speeds and power settings are designed to cover typical aircraft approach and takeoff operations. The rotors were configured in the test in a pusher configuration. The flow distortion created by the pylon was expected to increase the noise levels primarily for the front rotor. The influence of the pylon wake was mitigated through pylon edge blowing at conditions of interest, as detailed in Ref 2.

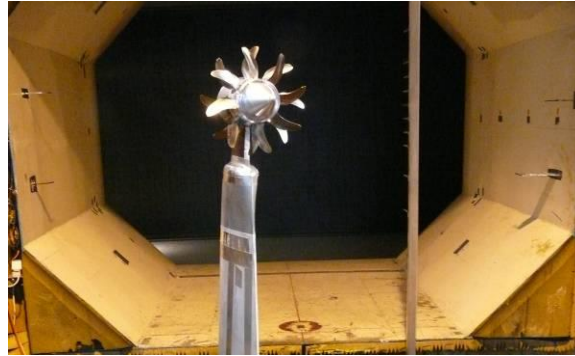


Figure 2. Isolated open rotor model in LSAF.

The BWB airframe planform model was manufactured at 8% scale of a 120-ft span demonstrator aircraft, as shown in Figure 3 with the open rotor installed in the test section of LSAF. The airframe model is derived from the BWB-450 airframe (Ref 10) and has NACA airfoils sections as leading and trailing edges. The maximum model chord is 60 inches and it is clipped in the span-wise direction to accommodate the model in the tunnel without excessive shear layer interference. A small part of the nose section is also clipped, as is evident in the photo shown in Figure 3. These modifications were done to accommodate the BWB model in the LSAF test section with a size that approximately match the 12-inch open rotor engine model, and were considered acceptable for the noise shielding study. For practical applications, the engines will likely be installed near the trailing edges of the airframe, to enable aerodynamic-propulsion integration. Thus, the fidelity of the airframe structure in the vicinity of the trailing edges near the engine installation critically controls the shielding characteristics, while the wing tips and the airframe nose section are not expected to noticeably affect the shielding.

Of course, the model modifications would affect the overall aerodynamic features if the effects of aircraft angle of attack were also considered in the study. Those effects would most noticeably manifest themselves in terms of changes in the incoming flows in front of the open rotor due to the circulatory flows associated with lifting surfaces and wings, potentially altering the noise source strengths. A simultaneous analysis of both the installation effects and the noise shielding effects is clearly very complicated and difficult. It may not be necessary and productive either, because the two are related to two different noise features, one on source changes and the other on shielding, which justifies the use of a planform airframe model in the test discussed here for noise shielding study, with the aircraft angle of attack set at zero degrees. As a result, the engine noise installation effects in such a setup are purely due to noise shielding by the airframe. In contrast, the study would be much more complex and expensive if the airframe model were a full configuration BWB model with the results including both the shielding effects and the flow effects due to the lifting body/wing. The former would reduce the engine noise under the aircraft due to shielding, while the latter would increase the engine noise due to inflow distortion. The two would compete to affect the radiated noise and it would be very difficult to separate one from the other.

Table 1. Rotor speeds in LSAF test (rpm).

<i>Front Rotor</i>	<i>Aft Rotor</i>
9000	10000
10800	12000
11700	13000
12600	14000
13500	15000
14400	16000

Since the shielding is mostly controlled by the geometry and design features near the engine installation, various local features were studied in the test to reveal their effects on noise shielding. These include vertical surfaces, trailing edge elevons and local surface liner treatments. Two different verticals were built for this model, each of which was tested at two different cant angles. The BWB airframe has the further capability to deflect the trailing edge elevons up and down by 5 degrees, simulating aircraft approach and takeoff operations. The BWB airframe also includes instrumentation panels in the main wing and the elevons where Kulite surface pressure sensors are embedded. These panels can be replaced with acoustic liner panels for three different liner designs. More detailed descriptions of these local features will be given in subsequent sections when discussing their respective noise shielding features.



Figure 3. BWB model with open rotors in LSAF.

The acoustic measurements in the test include both inflow and out-of flow microphones. In addition, surface Kulites and a phased array system were also used. The data acquired by out-of flow microphones suffered from the scattering effect of the tunnel shear layer that leads to a haystacking or broadening effect of the rotor tones. This effect increased with frequency and made the interpretation of tonal data challenging. Because of this, only the data from the inflow microphones will be discussed here. The inflow microphones were mounted on a traversing mechanism that allows microphone angles from 30 to 150 degree polar angles. A typical traverse would cover this range in 10 degree increments. Overall 13 microphones were mounted on a traversing sting covering azimuthal angles from +45 to -45 degrees relative to the open rotor horizontal. The microphones had B&K nose cones, type UA0385, to reduce flow noise.

Table 2. Brief summary of LSAF test matrix.

<i>Parameter</i>	<i>Unit</i>	<i>Variation</i>
Rotor Speed	rpm	Table 1
Mean Mach Number	-	0, 0.2, 0.24
Rotor Position in Flow Direction	<i>D</i>	-1, -0.5, 0, 0.25, 0.5, 0.75, 1, 1.5, 2
Rotor Position in Span Direction	<i>D</i>	0, 1.5
Rotor Position in Vertical Direction	<i>D</i>	0.685, 0.75, 1, 1.25
Angle of Attack	Deg	0
Vertical Tail Size	-	Large, Small
Vertical Tail Angle	Deg	102, 120
Elevon Angle	Deg	-5, 0, 5
Liner Type	-	Hook, Nomex, Straight

To establish a comprehensive database for open rotor noise shielding by BWB aircraft, the wind tunnel tests covered a wide range of parameters. These include various rotor speeds to simulate engine power settings at typical aircraft takeoff and landing operations, with corresponding mean flow conditions. The parametric variations also include the engine locations, in the flow direction in relation to the BWB trailing edge, in the span-wise direction on and off the BWB centerline, and in the vertical direction along the normal to the BWB upper surface. The BWB airframe variations include local design features such as vertical tails with two sizes and each at two cant angles and trailing edge elevons deployed for both takeoff and landing operations. In addition, the local airframe surfaces are also modified with acoustic liner treatments. The rotor speed variations are listed in Table 1 and the other parameters are summarized in Table 2, where the rotor position is measured at the rotor center with its diameter D as units. For variations in the flow direction, the position is in relation to the BWB trailing edge at the rotor installation span-wise locations with positive values for positions upstream of the trailing edge and negative values for downstream positions. For variations in the span-wise and the vertical direction, the positions are measured respectively in relation to the BWB centerline and its upper surface.

III. Directivity Patterns of Isolated Rotor Tones

Because of the legacy design of the open rotor model and the operating conditions used in the test, the overall noise characteristics of the wind tunnel test model can be expected to be different from those of more advanced and more recent designs. Open rotor technologies have advanced significantly in the past two decades and the noise levels of open rotor engines have been reduced so that it is feasible now to meet the aircraft noise regulations (Ref 4, 11). In addition to better blade design, current open rotors usually have smaller fan diameter and lower operating speed for the aft rotor, both of which help to reduce the loading on the aft rotor blades, and hence, reducing the amplitudes of interaction tones. The different blade designs and operating conditions will cause differences in noise spectral features and tonal energy distribution, and thus, differences in total noise characteristics. It is then natural to ask whether the database from the wind tunnel test with the legacy rotor design is relevant to the advanced engines, and how the database can be used in BWB shielding studies for general cases. To answer these questions, this section discusses the directivity patterns of the tones generated by the rotors, both the rotor tones and the interaction tones, and compares them with those representing more advanced designs. For noise shielding studies, the directivities are the noise features that affect the shielding efficiency; the absolute amplitudes are not relevant because the shielding effects are represented and applied as the differences in sound pressure levels. It should also be pointed out that for shielding studies, the directivities are important because of the edge diffraction effects; in cases where the edges of the scattering body are in the peak radiation direction, increased diffraction can be expected and the total shielding effects are jointly determined by the blocking of the sound propagation due to the BWB airframe and the diffraction by its edges.

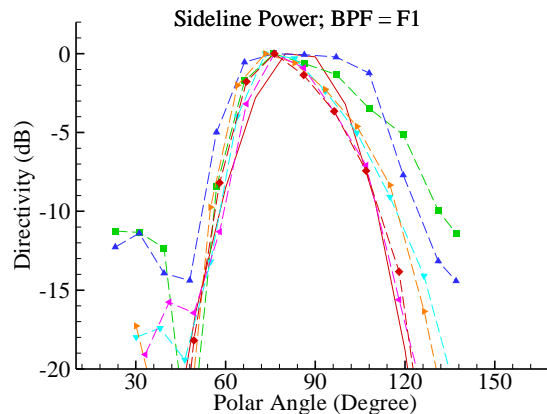


Figure 4. Directivities of front rotor BPF, F1, at takeoff power settings.

Examples of the directivity comparisons for isolated rotors are given in Figure 4 to Figure 6, shown as a function of the polar emission angle. The directivities are all normalized by their maximum levels so that they are all shown with maximum level of zero dB. In all the plots, the data are for typical takeoff power settings, but the trends are representative of other power settings. Each figure contains multiple cases, including speed and AOA variations, from the LSAF wind tunnel test, represented by the dashed curves with various types of symbols, and the typical directivity for more advanced rotor designs, given by the solid curves. All the wind tunnel data are normalized for a

mean flow Mach number of 0.24 with the rotor at zero degree angle of attack. Figure 4 plots the directivities for the tones at the front rotor Blade Passage Frequency (BPF). Similarly, Figure 5 plots the BPF tone directivities for the aft rotor. In both these cases, the tonal directivities show maximum radiation in the direction near the rotor plane, namely, at emission angles around 90 degrees, and the rotor tone noise falls off rapidly as the emission angle moves away from the peak radiation direction; the 10-dB down points usually only cover an angular domain of about 60 degrees around the peak emission angle, typically from 60 degrees to 120 degrees. It is clear from these figures that while there are some differences between the wind tunnel test dataset and the typical directivities of advanced designs, the main features of rotor tone radiation are consistently captured by the wind tunnel data.

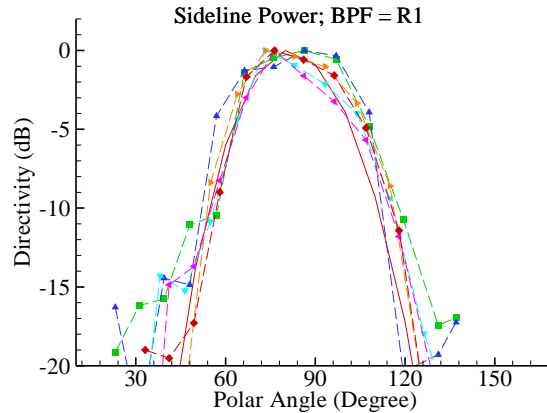


Figure 5. Directivities of aft rotor BPF, R1, at takeoff power settings.

Similar comparisons are given in Figure 6 for the first interaction tone of an isolated rotor. Again, the mean features of the tonal directivities are consistently seen in both the LSAF wind tunnel data and the advanced design, consisting of maximum radiations in the upstream and downstream directions and lower noise levels in a broad angular region in between. It can be seen that the wind tunnel test data have more scatter, mostly in the aft quadrant, and their agreement with the typical directivity of advanced open rotor design is not as good as the rotor tones shown in Figure 4 and Figure 5. This is probably expected because the interaction tones are more affected by the rotor design; differences in blade geometry and blade count, operating speed and rotor diameter may all affect the interaction tones, both their amplitudes and their directivities. Fortunately for noise shielding, these data scatter may only have a secondary effect. Due to practical constraints in aerodynamic-propulsion integration, engine installations for upper surface mounted configurations will likely be limited to the vicinity of the BWB airframe trailing edge. Thus, the aft quadrant in the downstream direction is not expected to benefit significantly from shielding, and the differences in the directivity patterns in the aft quadrant are expected to have minimal effects on the noise shielding.

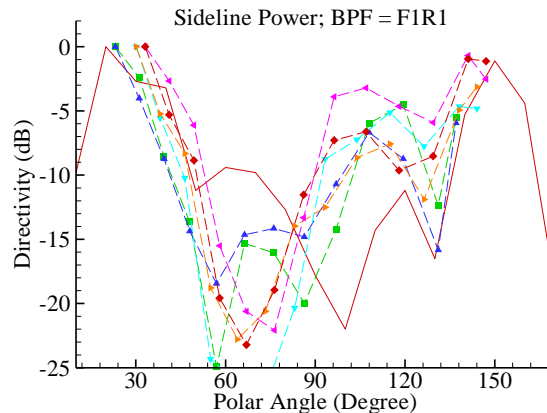


Figure 6. Directivities of the first interaction tone, F1R1, at takeoff power settings.

The above comparisons of the tonal directivities clearly show that the individual tones of the LSAF wind tunnel open rotor model have similar characteristics to what is expected for typical advanced open rotor designs. This, however, does not ensure the similarities in overall total engine noise, because the tonal amplitude distribution,

which critically controls the overall noise levels, is determined by the blade design, such as the number of blades for each rotor stage and the blade operating angles, and the rotor operating conditions including the power setting of each rotor stage. For example, two designs may have similar individual tonal directivities for the interaction tones, but if one of them is designed to operate at low aft rotor speed, this design will see less interaction tone noise, and thus, less radiation in the aft quadrant.

Because of this, the use of the wind tunnel test database in BWB shielding studies will not be as straightforward as that for turbofan engines dominated by broadband jet noise, where the matching of engine operating conditions between a particular run in wind tunnel tests and the full configuration application allows the shielding effects from that particular run to be directly applied, usually on the basis of 1/3 octave band sound pressure levels. In the case of open rotor noise shielding, the matching of engine power settings gives no guarantee that there will be the same number of tones within a particular 1/3 octave band and the tones will have matching or scalable amplitudes. Thus, the wind tunnel test database should be considered as a collection of tonal shielding effects for BWB noise shielding studies, and the shielding effects should be applied in full configuration applications on the basis of individual matching tones, as done in Ref 4. The tonal shielding effects, namely, tonal noise reduction, will of course depend on various flow, design and operating parameters, which are discussed in the following sections.

IV. General Shielding Characteristics

The general shielding characteristics can be intuitively understood by the principle of line-of-sight, or geometric acoustics, as illustrated in Figure 7 (Ref 8, 9). Noise shielding occurs when the acoustic waves from the sources cannot propagate directly to the observation point. With the engines mounted on the upper surface of the BWB airframe and the observation point on the lower side of the aircraft, significant shielding can be expected right below the engines, in the angular domain around the 90 degree emission angle below the aircraft. At large and small emission angles, especially at large angles in the aft quadrant in the downstream direction, acoustic waves can directly propagate to the observation point without any interactions with the airframe so that little shielding is expected in these regions. For distributed sources, as is the case for open rotors, there is a partially shielded angular domain between the shielded region and the insonified region where some acoustic waves can propagate directly to the observation point while some are blocked by the airframe, leading to partial shielding. In practical applications, the boundaries of these various regions will not be clear cut and abrupt, because the simple principle of line-of-sight only gives the first order effects and will be supplemented by the effects of sharp edge diffraction and possibly creeping wave radiation from large curved surfaces, leading to smooth transition from one region to another. Since there is no direct propagation in the shielded region below the aircraft, the noise levels there, namely, the shielding effect, are determined entirely by the diffracted waves, whose amplitudes are in turn determined by the source location in relation to the diffraction edges, as well as the source directivity and the source coherence. While the source location has been known to be an important parameter in acoustic shielding, the effects of source directivity and coherence have not been studied as much. The latter, however, plays a critical role in noise shielding of open rotor tones, and thus, will be discussed here.

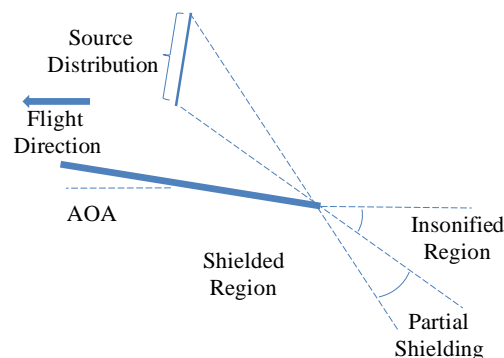


Figure 7. Illustration of general noise shielding characteristics.

Some examples of tonal shielding are shown in Figure 8 to Figure 10, plotting the difference in Sound Pressure Levels (SPL) between installed and isolated open rotors for individual tones. For the reasons discussed in the previous sections, the tones are grouped as front rotor tones shown in Figure 8, aft rotor tones in Figure 9 and interactions tones in Figure 10. The numerical values in the figures are the difference in SPL so that positive values correspond to noise increase and negative values represent noise reduction. The figures plot the shielding effects as a

function of the polar emission angle and tonal frequency, with the polar angles in the flyover plane. The results are for the case of mean flow Mach number of 0.24, rotor angle of attack of zero degrees, the front and rear rotor respectively at 14400 and 16000 revolutions per minute (rpm), which give a power setting for this rotor design corresponding to the typical aircraft takeoff operation power requirement, and the BWB model in its baseline configuration with elevons at zero deployment angle and no vertical tails and liner treatments. The center of the open rotor, defined as the mid-point between the forward and aft rotor, is located off the centerline of the BWB model in the span direction, one rotor diameter upstream of the BWB trailing edge in the flow direction and 0.75 diameters above its upper surface in the vertical direction. For easy reference, the key parameters for this baseline case are summarized in Table 3.

Table 3. Key parameters of baseline for discussion.

<i>Parameter</i>	<i>Unit</i>	<i>Value</i>
Mach Number	-	0.24
Angle of Attack	Deg	0
Front Rotor Speed	rpm	14400
Aft Rotor Speed	rpm	16000
Rotor Center to TE	<i>D</i>	1
Rotor Center to BWB Centerline	<i>D</i>	1.5
Rotor Center to BWB Surface	<i>D</i>	0.75
Elevon Angle	Deg	0
Vertical Tail	-	none
Surface Liner	-	none

From the engine installation geometry, it is easy to calculate the angular boundaries of the various regions defined in Figure 7. In the aft quadrant, the boundary for the shielding region for the front rotor tones is about 131 degrees, below which significant shielding can be expected and beyond which the shielding efficiency can be expected to decrease. This is clearly seen in Figure 8, where a transition from the heavily shielded region of up to 20 dB noise reduction to a more moderate reduction of about 6 dB is seen at about 130 degrees of emission angle, almost uniformly for all the frequencies. As the emission angle increases further in the downstream direction, the shielding effects gradually decrease as the insonified region is approached. In the upstream direction in the forward quadrant, the shielding region boundary is less well defined. If the local wing chord length is used to calculate the shielding angle, the angular boundary is at about 30 degrees, which is at the lowest data point shown in Figure 8, and thus, makes the entire forward quadrant shown in this figure the shielded region. However, the BWB model has a highly swept leading edge, as can be seen in the photo in Figure 3. Thus, the edge diffraction can significantly increase the noise levels in the shielded region, which is probably why the noise reduction at emission angles up 50 degrees is only about 5 dB, even though these angles are in the shielded region, and the amount of noise reduction is not uniform in frequency, due to the interference effects of the diffracted acoustic waves. It can also be seen that in the shielded region under the aircraft, around the overhead direction of 90 degrees, for example, the amount of noise reduction generally increases with frequency, which is a well-known feature of acoustic wave scattering; for waves from sources at fixed locations, the higher frequency waves have shorter wavelength, leading to less diffraction in the shielded region.

From the discussions in the previous section, the aft rotor tones are known to have similar directivities to those of the front rotor tones, and therefore, similar shielding effects might be expected. The comparison between Figure 8 and Figure 9, however, reveals noticeable differences between the two groups of rotor tones; the amount of noise reduction is smaller and the angular shielded region is narrower for the aft rotor tones. This can be explained by the axial separation distance between the two rotors; if the tone sources are assumed to be located at the rotor faces, the aft rotor tones are generated at a distance downstream of the front rotor, equal to approximately 20 percent of the rotor diameter. This defines the aft rotor shielding angle at about 126 degrees, compared with 131 degrees for the front rotor.

In the respective shielded zones of the two groups of tones, the noise reduction is noticeably different, with the aft rotor tone noise reduction smaller by more than 6 dB for the low and intermediate order tones. The smaller distance between the rotor location and the BWB trailing edge for the aft rotor tones may contribute to the smaller noise reduction of the aft rotor tones in the shielded region, but a large part of the noticeably smaller shielding

effects is most likely due to the highly directional nature of the tonal noise. With the slight shift of the source location in the downstream direction, by about 20 percent of the rotor diameter, the diffracted field of the aft rotor tones is about 2 dB higher than that of the front rotor, due to the less spherical spreading of the sound propagation away from the source. The source location shift will also cause an increase in the diffracted field by effectively putting the trailing edge at an emission angle closer to the peak radiation angle of the tone directivity, by about 5 degrees. Since the rotor tone directivities are highly directional with rapid amplitude changes, as analyzed in the previous section, a shift of about 5 degrees in emission angle can lead to a large change in amplitude. From the results shown in Figure 5 for the first aft rotor tone, the slope of the directivity curves at about 120 degrees can be estimated to be -1.4. Thus, a shift of 5 degrees towards the peak radiation angle would correspond to an increase of amplitude of about 7 dB. This, together with the increase due to the shorter distance, can explain the much smaller shielding effects of the aft rotor tones.

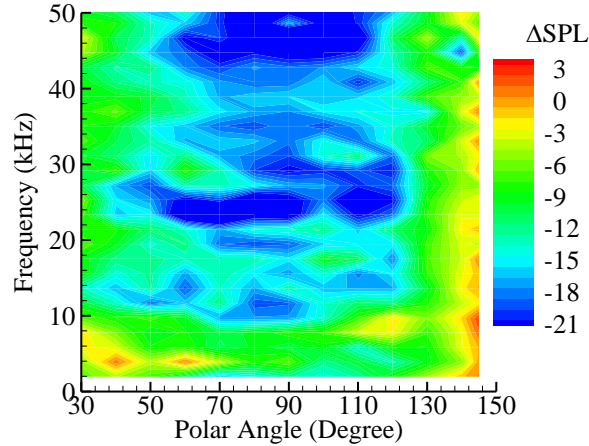


Figure 8. Shielding effects in the flyover plane for front rotor tones at takeoff power.

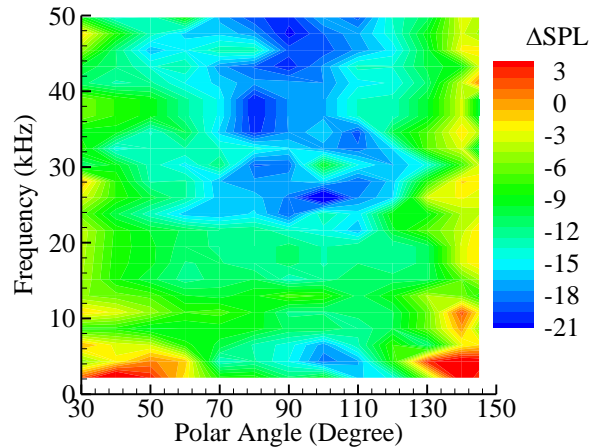


Figure 9. Shielding effects in the flyover plane for aft rotor tones at takeoff power.

It is known that the major noise generation mechanism for open rotor interaction tones is the interaction of the unsteady wake flows from the front rotor blades with the aft rotor blades. Thus, the noise sources can be considered as being located at the aft rotor face and having a high degree of incoherence due to the incoherent features of the turbulent wake flows. From the source location, the size and boundaries of the shielded zone of the interaction tones can be expected to be similar to those of the aft rotor tones, as is clearly seen in Figure 10 which plots the shielding effects on interaction tones. The heavily shielded region of noise reduction of more than 20 dB is bounded in the downstream direction at about 125 degrees, consistent with the shielding angle estimated by the aft rotor location. By comparing the results for the interaction tones with those for the rotor tones, a striking feature is that the interaction tone shielding shows much less dependency on frequency and on emission angle than the rotor tones; the shielding zone boundaries in Figure 10 are roughly at constant emission angles and the amount of noise reduction is

almost uniform in frequency, in contrast to Figure 8 and Figure 9 where the noise reduction increases with frequency in the shielded regions. The frequency dependent shielding of the rotor tones can be explained by the well-known feature of acoustic scattering by sharp edges for simple coherent sources. The rotor tones are due to the loading on and the thickness effects of the rotating blades, which furnish highly coherent sources for the radiated tonal noise. On the other hand, the sources of interaction tones are postulated to be much more incoherent, resulting from the incoherent turbulent wake flows behind the front rotor, which of course leads to an incoherent diffraction in the shielded region where the noise originates from a set of mutually independent sources along the edges of the BWB airframe without much interference between them.

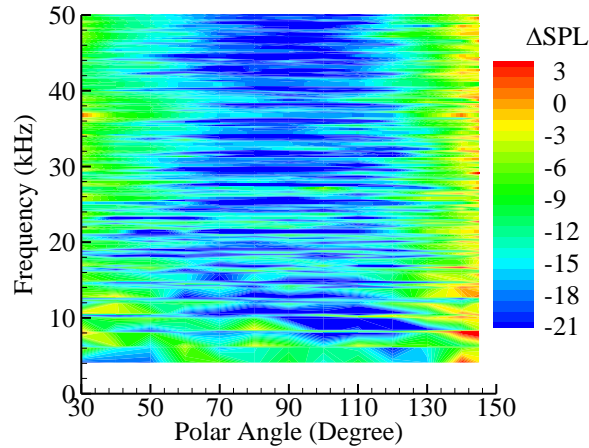


Figure 10. Shielding effects in the flyover plane for interaction tones at takeoff power.

While acoustic scattering and diffraction of simple, perfectly coherent, and omnidirectional sources by sharp edges has been extensively studied in the past, the effects of distributed sources with highly directional directivity and low coherence have not attracted as much attention. These are important characteristics of open rotor tonal sources and are postulated here to have lead to the significantly different shielding effects for the three groups of tones. It is appropriate to point out that this is postulated here as a potential explanation of the test data and more studies are needed to conclusively prove/disprove the mechanisms.

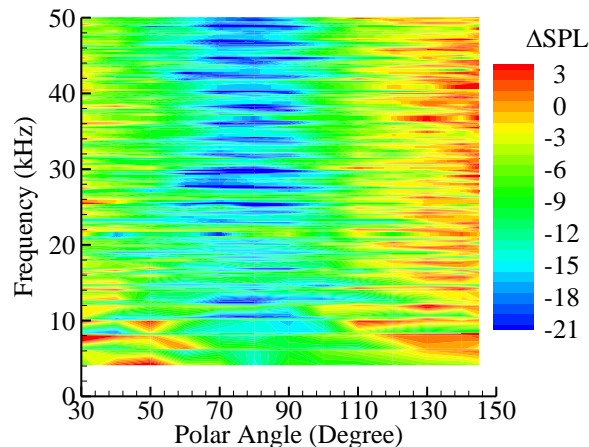


Figure 11. Shielding effects at sideline locations for interaction tones at takeoff power.

The results shown in Figure 8 to Figure 10 and the discussions associated with the results in the previous paragraphs are for emission angles in the flyover plane right below the aircraft, in which the shielding characteristics are mostly determined by the local geometry at the span-wise location of the engine installation, similar to two-dimensional scattering. The flyover plane can be expected to be the maximum shielding azimuthal angle because of the large blocking effect of the BWB airframe. At sideline directions, the shielding benefit is usually smaller because of the smaller effective chord length of the blocking wing in the sideline direction. The details of the shielding patterns and the amount of noise reduction of course depend on the detailed design of the airframe, the

sweep angle and the taper factor of the wing, for example. For the BWB airframe tested in LSAF, shown in the photo in Figure 3, the wing is highly swept, significantly reducing the effective shielding surface length, and the trailing edge curves in the upstream direction, effectively exposing the engines to a large angular domain of emission angle without any benefit of shielding. As a result, the BWB has much less shielding benefit for sideline directions than the flyover plane. This is illustrated in Figure 11, which plots the shielding effects of interaction tones in the sideline direction at an azimuthal angle of 45 degrees away from the flyover plane. The figure is in the same format and for the same operating conditions as in Figure 10, all summarized in Table 3, which facilitates the comparisons of the two cases.

The similarity between the two figures is that the shielding characteristics analyzed above are all clearly revealed in the sideline direction, including the shielding patterns and the amount of noise reductions, and the almost frequency independent scattering of the interaction tones due to the incoherent nature of their sources. The major difference between the two figures is the significantly smaller shielding effects at the sideline direction. In comparing the two figures, it is easy to see that the shielded region at the sideline direction is greatly reduced, by as much as 20 degrees in the downstream direction from about 130 degrees of emission angle to about 110 degrees. This will leave a large part of the aft quadrant exposed to direction radiation from the engines, significantly diminishing the benefit of the BWB noise shielding. Within the shielded regions, the amount of noise reduction is also significantly less, by about 10 dB, compared with the flyover direction. However, this may be less of a concern in practical applications, compared with the reduced shielded area, because the reduction in the shielded regions is still at least 6 dB. Thus, further noise reduction in this case needs to focus more on the aft quadrant, where the BWB shielding has very limited effects.

V. Effects of Engine Locations

As discussed in the previous section, the engine installation position in relation to the BWB airframe trailing edge is one of the most important parameters controlling the shielding characteristics. It not only sets the size of the shielded zones, and hence, the amount of propagation blocked by the BWB airframe, but also determines the level of the diffracted field in the shielded regions. The amount of noise reduction is also impacted by the propagation distance from the sources to the scattering edges and by the directivity effects that control the amount of acoustic energy incident on the edges and diffracted into the shielded regions. These effects are illustrated in Figure 12 and Figure 13, which, together with Figure 10, show the effects of variations in rotor location from being right at the BWB trailing edge (Figure 12) to $1D$ upstream of it (Figure 10), and then to $2D$ upstream of it (Figure 13), where D is the rotor diameter. The configuration definitions for the results in these features are listed in Table 3. The center of the open rotor is located off the centerline of the BWB model in the span-wise direction, and at 0.75 diameters above the airframe surface in the vertical direction. The figures plot the shielding effects of the interaction tones, but the parametric trends on the engine locations are representative of the rotor tones.

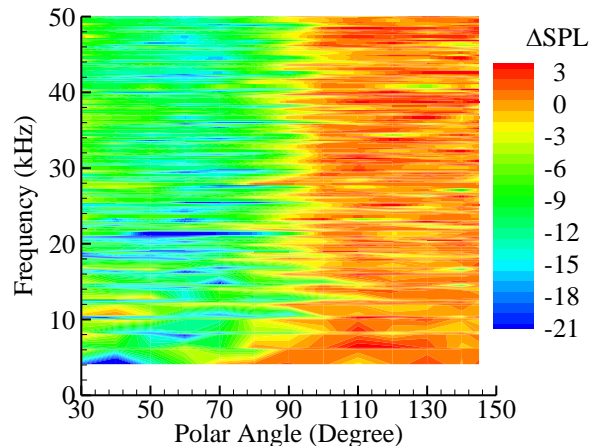


Figure 12. Shielding effects of interaction tones with rotor center at trailing edge.

Figure 12 is for the case with the center of the open rotor located at the BWB trailing edge, radiating noise unobstructed into the aft quadrant and having all the noise blocked in the forward quadrant. This is clearly shown in the figure by the divide between the shielded region and the insonified region at the emission angle of 90 degrees. As analyzed in previous sections for the case of interaction tones, the shielded zone is well defined and the shielding

amplitude patterns are essentially uniform in frequency. It is interesting and important to note that the insonified zone in the aft quadrant has a slight increase in noise levels due to the extra noise from the trailing edge diffraction. Since the interaction tones are highly incoherent, the extra noise component always causes an increase in noise levels because its contribution is added to the total noise on the energy basis. As the engine moves upstream to the upper side of the BWB airframe, noise shielding expectedly increases, very significantly for the case of the rotor being at two rotor diameters upstream of the BWB trailing edge, as shown in Figure 13. In this case, the entire domain of emission angles from about 30 to 150 degrees is in the shielded zone with large noise reduction of more than 20 dB.

Each of the cases shown in Figure 10, Figure 12 and Figure 13 has its own shielded zone determined by the respective rotor position relative to the trailing edge. The boundaries of the shielded zones can be predicted by the principles of geometric acoustics, which are listed in Table 4 for all the cases tested in LSAF. This is only for the downstream boundaries of the shielded zones; as discussed in the previous section, the upstream boundaries of the shielded zones are less well defined due to the highly swept BWB leading edge. In practical applications with the engines mounted near the airframe trailing edge, the upstream boundaries are less critical because of the small emission angles associated with the upstream shielded zone boundary and the usually significant shielding effects in the forward quadrant. It is interesting to note that these shielded zone boundaries calculated by simple geometric acoustics are well revealed by the data plotted in the figures. The agreement is very good for all the engine locations, both upstream and downstream of the trailing edge. As discussed in the previous section, the axial spacing between the front and the aft rotor yields a difference in the shielded zone, usually by a few degrees, as can be seen in Table 4. Since the interaction tones are generated mostly at the aft rotor location, the last column in the table should be relevant to the results shown in the figures.

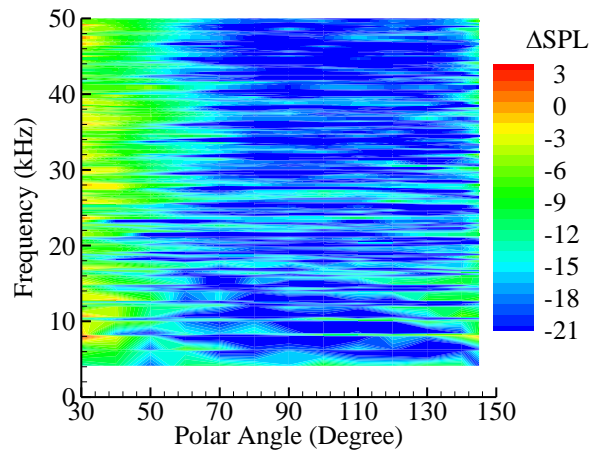


Figure 13. Shielding effects of interaction tones with rotor center 2D upstream of trailing edge.

The analyses and discussion in this section and the previous section are done with representative examples of the LSAF test database to illustrate the major trends. The selection of representative examples is also influenced by the large amount of data and the large number of figures that would be needed to show all the tonal shielding effects, especially with the large number of parameters covered in the study, both in this section and the subsequent sections. Thus, it is of interest to define a simpler metric which can reveal the qualitative trends for the understanding of the shielding effects, even though the simple metric may not be suitable for quantitative calculation and prediction of the shielding effects. To this end, the noise reduction due to shielding effects is averaged in frequency, reducing one parameter in the database. With this, the results shown in the form of contour maps in previous figures are reduced to one directivity curve per diagram. For the effects of engine location in the flow direction on the interaction tones, the data can now be presented in a set of curves as shown in Figure 14, which plots the frequency averaged noise reduction due to shielding as a function of the emission angle, with each curve representing a rotor position, as indicated on the curves with the rotor diameter D as the unit. The rotor position is measured in relation to the BWB trailing edge, with positive values for positions upstream of the trailing edge and negative values for downstream positions.

Table 4. Prediction of shielded zone boundaries in emission angle (Deg).

<i>Rotor Center</i>	<i>Front Rotor</i>	<i>Aft Rotor</i>
---------------------	--------------------	------------------

$-1D$	54	49
$-0.5D$	72	64
$0D$	95	85
$0.25D$	106	97
$0.5D$	116	108
$0.75D$	124	117
$1D$	131	126
$1.5D$	142	138
$2D$	149	147

The major trends of the shielding effects due to rotor positions in the flow direction can now be easily seen and discussed from Figure 14, for the flyover plane ($\phi = 90^\circ$). Starting with the case of the rotor located one diameter downstream of the trailing edge, it is clear that the BWB shielding in this case is confined to a narrow zone in the forward quadrant, below about 50 degrees, which is clearly shown in Figure 14 and accurately predicted in Table 4. The shielding levels are moderate and there is a slight noise increase in the insonified region. As the rotor moves upstream in the flow direction, the shielded zone expands and its boundary shifts in the downstream direction. The positions of the shielded zone boundary are all well predicted in Table 4. As the shielded zone expands, the levels of noise shielding inside the zone gradually increase, from a few dB in the case of the rotor behind the trailing edge to more than 20 dB when the rotor is two diameters upstream of the edge.

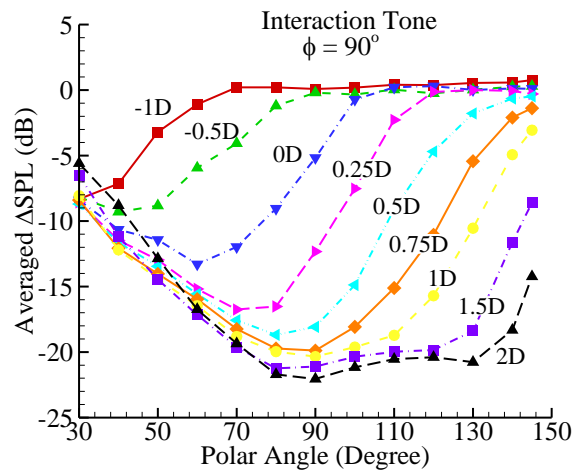


Figure 14. Shielding on interaction tones at various rotor positions in flow direction.

The rotor location in the vertical direction normal to the BWB upper surface may also have an impact on the shielding levels. This is illustrated in Figure 15, where the shielding effects on the interaction tones in the flyover plane are shown for various rotor positions in the vertical direction, defined to be the distance between the rotor center and the airframe surface. The test model configurations and the operating conditions are listed in Table 3. There are two groups of curves plotted in Figure 15, respectively for the stream-wise rotor location of one and 0.5 rotor diameter upstream of the trailing edge. Obviously, the group of curves with higher levels, less shielding, is for the $0.5D$ case and the other set with lower levels is for the $1D$ case. In each group, results are shown for four rotor heights, as indicated in the figure. By comparing the curves within a group, it is clear that the effects of rotor height on the shielding levels in the forward quadrant are small, as would be expected because the leading edges of the BWB airframe is far away from the rotor tone sources. In the aft quadrant at large emission angles, however, noticeable effects can be seen, up to 5 dB in some cases from a rotor height of one diameter to $2/3$ of a diameter. The general trend is that as the rotor moves closer to the BWB upper surface, the shielded zone expands because more emission angles are blocked by the airframe, and hence increasing the shielding effects.

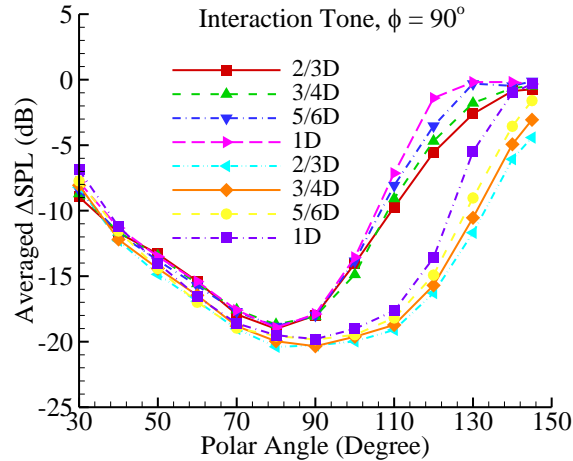


Figure 15. Shielding on interaction tones for various rotor positions in vertical direction.

The quantitative results and analyses in this section have shown the significant impact of rotor positions on noise shielding, which have also illustrated the huge potential of noise reduction by acoustically optimizing the airframe/rotor integration, which is one of the motivations of the BWB aircraft with upper surface mounted engines. In practical applications, it should be realized that the engine installation is subject to many other constraints, of which the most important is the aerodynamic propulsion integration that dictates the stream-wise position of the engines. This requires the engines to be kept out of the high speed flow region on the upper side of the airframe at cruise conditions, both to maintain the aerodynamic performance of the lifting wings and to ensure the propulsion efficiency of the engines. With currently available technology, engines installed about one rotor diameter upstream of the BWB trailing edge may be able to meet this integration requirement, but positions further upstream would pose a very difficult technical challenge. The choice of engine installation height should also be balanced between the acoustic benefit of a low engine height, as illustrated in Figure 15, and other factors, of which the most important is probably the injection of turbulent boundary flows on the BWB airframe surface into the rotor inflow. This may occur when the aircraft is at large angles of attack, as the BWB is designed to operate and the resulting thicker boundary layer flows at these operating conditions. In this case, the inflow distortion can significantly increase the levels of the tonal noise sources, and even more importantly, significantly degrade the efficiency of the rotor operation.

VI. Effects of Vertical Tails

As discussed in the previous sections, noise shielding by the BWB aircraft is not very efficient at sideline locations, both because of the small chord length at the sideline direction and due to the leading edge sweep and curved trailing edge of the BWB airframe. It is then of interest to look for devices and design features that can enhance the sideline shielding. Vertical tails are one of the natural candidates; they are usually installed on the side of the engines, and thus, can be expected to block the acoustic wave propagating in the sideline direction, and they are multi-function components, also used for stability control. The acoustic effects of the vertical tails are illustrated in Figure 16, which plots the shielding on interaction tones in the sideline direction 45 degrees from the flyover plane. The test configurations are defined in Table 1, with one of vertical tails, the V1 design, installed at 120 degrees of cant angle, as shown in the photo in Figure 3. The results in Figure 16 are to be compared with Figure 11, which clearly reveals the impact of the vertical tails; the shielded zone is widened and the level of noise reduction is increased. For example, if the edges of the blue color zones in the figures are used as a measure of the shielded zones, the shielded zone without the vertical tails is approximately from 55 to 100 degrees, while that with the vertical tails is from 50 to 115 degrees, a significant increase of the blockage area.

The overall effects of the vertical tails on sideline shielding are also illustrated in Figure 17, including all four configurations with vertical tails, consisting of two sets of vertical tails respectively deployed at two cant angles. The two sets of vertical tails are named V1 and V3, with the former differs from the latter in its larger height, by approximately 50 percent. The two cant angles are respectively 102 and 120 degrees, with the cant angle of 90 degrees corresponding to perpendicular to the airframe surface. For comparison, the case without vertical tails is also plotted in the figure by the black solid curve, while the cases with vertical tails are plotted as various broken curves with symbols. There is only a small difference between the two sets of vertical tails and the two deployment

angles, on the order of one dB, with the best in the set, for interaction tones, being the V3 design at 102 degrees of cant angle, shown by the lowest curve in the figure marked by the inverted blue triangles. The comparison with the case without vertical tails, however, reveals significant increases in shielding effects, about 3 dB in the forward quadrant and up to 8 dB for some of the emission angles in the aft quadrant. These additional shielding effects mostly come from the blocking of the propagation area left open by the curved trailing edges, towards the upstream direction.

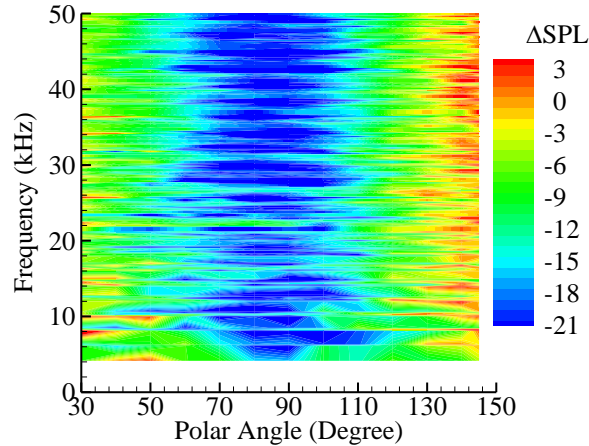


Figure 16. Shielding on interaction tones in sideline direction with V1 at 120 degrees.

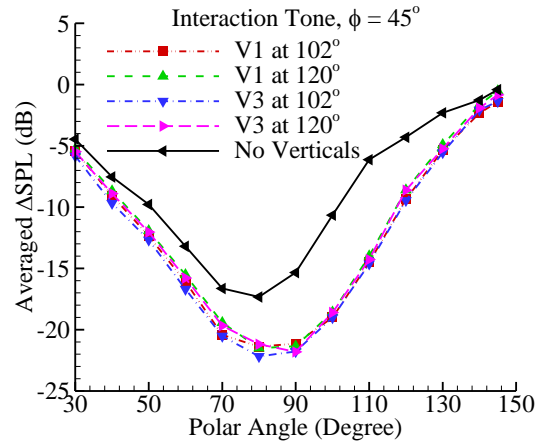


Figure 17. Effects of vertical tails on interaction tone shielding in near side direction.

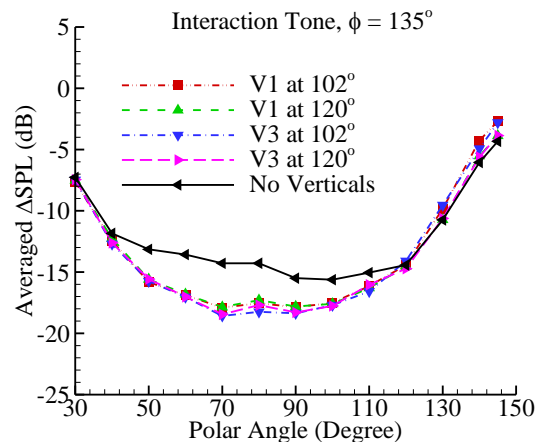


Figure 18. Effects of vertical tails on interaction tone shielding in far side direction.

The results shown in Figure 16 and Figure 17 are for the sideline angle of 45 degrees, namely, 45 degrees from the flyover plane on the side of the aircraft where the open rotor is close to one of the two vertical tails. This side is named the near side direction in Figure 17. Sideline noise measurement of course also includes the opposite direction, at 135 degrees, for which the rotor is located further away from the other vertical tail in the span-wise direction, named as the far side direction in Figure 18. Viewed from the measurement location, the former is the case of a rotor hiding right behind a large blocking surface, and thus, can be expected to have better shielding effects, in comparison with the latter where the blocking angle is smaller because of the larger distance between the source and the blocking surface. This is shown by Figure 18, which plots the shielding results for the same conditions as in Figure 17, but with the measurements at 135 degrees of sideline angle, exactly the opposite side to that for Figure 17. In this case, the enhancement of the shielding effects by the verticals is much smaller, in the sense that the additional noise reduction due to the vertical tails is all confined to an angular domain in which the noise has already been heavily shielded by the BWB airframe without the vertical tails, from about 50 to 100 degrees. This would make the impact to the total aircraft noise at these locations hardly noticeable.

It is also important to note that there is an increase of up to about 2 dB in noise levels due to the vertical tails at large emission angles in the aft quadrant, approximately above the angle of 120 degrees. This is due to the reflection from one of the two vertical tails that is located right behind the rotor, viewed from the measurement location at a sideline angle of 135 degrees. This is a double effect of a vertical tail; it is a blocking surface for one side of the aircraft and a reflection surface for the other side. In addition, in the flyover plane, the shielding effects of the vertical tails will be absent while the reflections may increase the noise, by the mechanism similar to megaphones. Thus, the resultant acoustic effects of vertical tails are by no means guaranteed to be beneficial, as clearly demonstrated in Ref 4, and should be studied on the aircraft system level with considerations for the detailed designs and component noise source levels.

VII. Effects of Surface Liner Treatments

An acoustic liner is a proven noise reduction technology widely used inside turbofan engines, usually deployed on the engine casing walls. It is known to be very efficient for tone dominated noise field. For the open rotor engines that are tone dominated, there is no engine casing to apply this treatment in the conventional manner, and the innovation of Ref 2 is to utilize the airframe surfaces in the vicinity of the engines for the deployment of the liner treatment. It should be acknowledged up front that this can be a radical and aggressive idea that is against the principle of aerodynamic design; the airframe surfaces are all exposed to external aerodynamic flows and thus are to be designed with minimum drag for aerodynamic efficiency. Currently available liner treatments all induce drag, equivalent to converting smooth surfaces to roughness surfaces, making this concept unfeasible for current applications. Thus, to make liner treatment practical for external airframe surfaces, new technologies will have to be developed for low-drag or drag-less liners. In this section, the acoustic effects of surface liners are presented, both to demonstrate the acoustic potential of this concept and to quantify the benefits. The latter can hopefully be used to guide the decision making in developing this technology in the future.

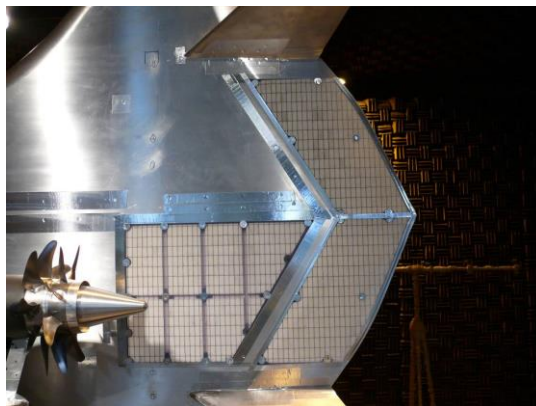


Figure 19. BWB model with local liner treatments.

For the BWB configurations studied here, the engines are located near the BWB trailing edge. Thus, the liner treatment can be deployed in the vicinity of the engines on both the main wings and the elevons. This is illustrated in Figure 19, where the surface areas with grid-like structures are the locations for the liner treatments. To test the noise reduction efficiencies of various liner designs, three types of liner were tested; they are Straight Liner, Hook

Liner and Nomex Broadband Liner, all of which were designed by the NASA Langley Liner Technology team specifically for the LSAF open rotor experiment. The liners were designed for peak attenuation of frequencies from 1BPF to 2BPF. Three engine locations were tested for the acoustic liner, respectively at $1D$, $1.5D$ and $2D$ from the BWB trailing edge. These relatively large distances from the engines to the BWB trailing edge allow sufficient space for the interactions between the sound waves and the treated surfaces; obviously, if the engines are very close to the trailing edge, the sound waves can mostly propagate directly from the rotors to the far field without interacting with the surfaces, rendering the liner treatment ineffective. For all the cases, the V1 vertical tails are installed at 120 degrees for the liner tests. This is a necessary design choice when considering surface treatment, because without the verticals, the waves impinging on the airframe surface would be reflected upwards, becoming irrelevant to the noise on the ground. In other words, the potential effects of the surface liner can be expected to be confined only to the sound waves that also hit the verticals.

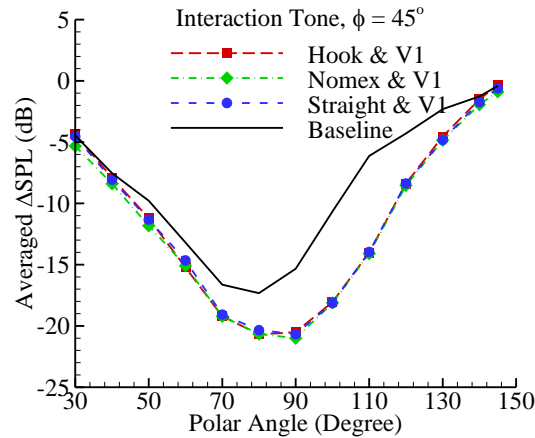


Figure 20. Effects of liner and vertical tails on near side shielding of interaction tones.

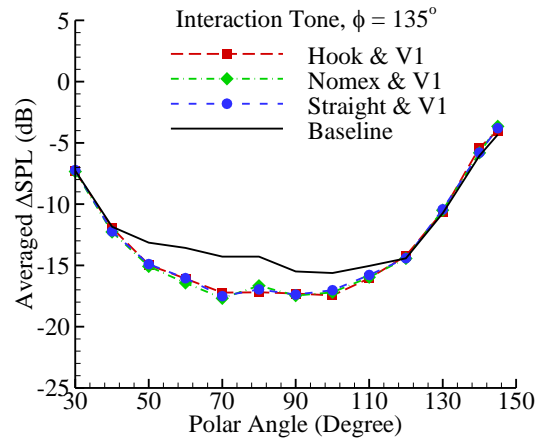


Figure 21. Effects of liner and vertical tails on far side shielding of interaction tones.

The combined effects of liner and vertical tails are illustrated in Figure 20 and Figure 21 for interaction tones, respectively for the near side and far side direction, with other conditions listed in Table 3. Both figures show that the effects of liner type are very small, with variations between the symbols within one dB. For comparison, the case without the liner and vertical tails is plotted in the figures by the black solid curve. The results show that the shielding is enhanced from the baseline case in both the near side and the far side direction. The enhancement is, however, mostly due to the vertical tails. It is interesting to compare Figure 20 with Figure 17, the latter being the effects of the vertical tails alone with the curve marked by the green triangle symbols representing the V1 vertical tail configuration discussed here. It can be seen that the two figures are essentially the same, indicating that the liner effects are negligible for this case. This is actually not a surprise; the near side direction experiences the large additional shielding due to the vertical tails, and the diffracted waves in the shielded zone on this side of the aircraft do not even hit the liner surfaces that deployed on surfaces facing the rotor. Thus, the liner effects are expected only

on the far side direction where the reflections from the vertical tails are an extra noise contributor, which is the cause for the noise increase in the aft quadrant, analyzed in the previous section and shown in Figure 18. This figure can be compared with Figure 21 and it is clear that the extra noise due to the vertical tail reflection in the aft quadrant is suppressed by the liner so that the noise levels for the liner treated cases become about the same as that for the baseline case, as if the reflections were not there.

VIII. Conclusions

To understand the noise shielding characteristics of BWB aircraft with open rotor propulsion and to provide data for BWB aircraft system noise assessment and prediction tool development, this paper has presented a study on the parametric trends of tonal shielding features, using a model scale open rotor simulator and a simplified BWB airframe planform model. It has been shown that the three groups of tones, namely, the front rotor tones, the aft rotor tones and the interaction tones, have very different shielding characteristics, due to differences in their respective tonal directivity, source location and source coherence, which lead to different sizes of the shielded zones, different levels of noise reduction in the shielded zones, and different shielding patterns in emission angle and frequency. Thus, it has been proposed that the study of open rotor noise shielding and the application of the shielding data for noise prediction for full configuration aircraft needs to follow the tonal approach which categorizes the tones into the three groups and applies the noise suppression on the individual tones. This paper has also presented various functional trends of the shielding effects on parameters covering rotor operations, BWB airframe designs and surface liner treatments, both quantitatively with detailed tonal noise suppression levels as a function of frequency and emission angle, and qualitatively in terms of a frequency averaged shielding metric. The latter has been used to reveal the shielding characteristics, while the former can and will be used to further develop parametric models for the prediction of shielding effects of open rotor noise.

Acknowledgments

The authors thank the NASA Environmentally Responsible Aviation Project, Dr. Fay Collier, Project Manager, for funding this research.

References

1. Harris, R.W., and Cuthbertson, R.D., "UDFTM/727 Flight Test Program," AIAA Paper 87-1733, 1987.
2. Czech M., and Thomas, R.H., "Open Rotor Aeroacoustic Installation Effects for Conventional and Unconventional Airframes," 19th AIAA/CEAS Aeroacoustics Conference (Berlin, Germany), American Institute of Aeronautics and Astronautics, Reston, VA, 2013, (submitted for publication).
3. Thomas, R.H., Burley, C.L., Lopes, L.V., Bahr, C.J., Gern, F.H., and Van Zante, D. E., "System Noise Assessment and the Potential for a Low Noise Hybrid Wing Body Aircraft with Open Rotor Propulsion" ,52nd Aerospace Sciences Conference (National Harbor, MD), American Institute of Aeronautics and Astronautics, Reston, VA, 2014.
4. Guo Y. and Thomas, R.H "System Noise Assessment of Blended-Wing-Body Aircraft with Open Rotor Propulsion" SciTech 2015, American Institute of Aeronautics and Astronautics, (submitted for presentation).
5. Bonet J. T., Schellenger H. G., Rawdon B. K., Elmer K. R., Wakayama S. R., Brown D. & Guo Y. P. "Environmentally Responsible Aviation (ERA) Project – N+2 Advanced Vehicle Concepts Study and Conceptual Design of Subscale Test Vehicle (STV)," NASA Contract NND11AG03C Report, December 2011.
6. Thomas R. H., Burley C. L. & Olson E. D., "Hybrid Wing Body Aircraft System Noise Assessment with Propulsion Airframe Aeroacoustic Experiments," *International Journal of Aeroacoustics*, Vol. 11 (3+4), pp. 369-410, 2012.
7. Czech M. J., Thomas R. H. & Elkoby R., "Propulsion Airframe Aeroacoustic Integration Effects of a Hybrid Wing Body Aircraft Configuration," *International Journal of Aeroacoustics*, Vol. 11 (3+4), pp. 335-368, 2012.
8. Dowling A. P. and Ffowcs Williams J. E. 1983 *Sound and Sources of Sound* Ellis Horwood Publishers.
9. D. G. Crighton, A. P. Dowling, J. E. Ffowcs Williams, M. Hekle and F. G. Leppington, *Modern Methods in Analytical Acoustics*. Springer-Verlag, 1992.
10. Liebeck, R.H., "Design of the Blended-Wing-Body Subsonic Transport," AIAA Paper No. 2002-0002.
11. Van Zante, D.E., "The NASA Environmentally Responsible Aviation Project / General Electric Open Rotor Test Campaign," AIAA Paper 2013-415, January, 2013.